An automated 55 GHz cryogenic Josephson sampling oscilloscope

Bodin, P.; Jacobsen, M. L.; Kyhle, Anders; Hansen, Jørn Bindslev; Davidson, A.; Brady, M.; Olsen, L.; Qualmann, Werner

Published in:
Review of Scientific Instruments

Link to article, DOI:
10.1063/1.1144233

Publication date:
1993

Document Version
Publisher's PDF, also known as Version of record

An automated 55 GHz cryogenic Josephson sampling oscilloscope

P. Bodin,[a] M. L. Jacobsen, A. Kuehle, and J. Bindslev Hansen
Physics Laboratory I, Technical University of Denmark, Bldg. 309 DK-2800 Lyngby, Denmark

A. Davidson and M. Brady
IBM Research Division, T. J. Watson Research Center, Yorktown Heights, New York 10598

L. Olsen and W. Qualmann
Physics Laboratory I, Technical University of Denmark, Bldg. 309 DK-2800 Lyngby, Denmark

(Received 9 June 1992; accepted for publication 23 September 1992)

A computer-automated superconductive 55 GHz sampling oscilloscope based on 4 kA/cm^2, $Nb/Nb_2O_5/Pb$ edge Josephson junctions is presented. The Josephson sampler chip was flip-chip bonded to a carrier chip with a coplanar transmission line by use of a novel flip-chip bonding machine. A 5.6 ps step pulse was successfully coupled in to the transmission line and 18.5 GHz multiple reflections plus a parasitic oscillation at 43 GHz were observed.

I. INTRODUCTION

For about ten years Josephson sampling oscilloscopes have been used in a wide range of cryogenic experiments to observe electronic signals with microampere amplitude and picoseconds rise time.[1-4] As the result of a collaboration between IBM Research Center, Yorktown Heights and Physics Laboratory I, The Technical University of Denmark we now have a computerized 2–55 GHz sampling oscilloscope with a sensitivity of about 1 μA. The measurement data are stored as sequential files and postprocessing is possible with a variety of programs. The oscilloscope sampling head employs hysteretic superconducting Josephson Junction circuitry[9,10] operating at 4.2 K for both the sampling gate and the strobe pulse generator. Using a cryogenic sampling head reduces thermal noise at low temperatures; using superconducting materials allows a higher bandwidth in the measurements, since the resistive losses are very low up to the gap frequency of the superconductor (in this case about 700 GHz).

While Josephson samplers are usually integrated on the experimental chip,[5-8] this procedure only allows measurements on the components on the experimental chip itself. In this work we have made an external connection to the sampler chip by means of the flip-chip bonding technique[11] in order to use the sampler as a multipurpose cryogenic instrument.

Figure 1 shows the 6×6 mm^2 silicon sampler chip (SC) connected face to face with a 1×1 in.^{2} sapphire carrier chip (CC). The surface of the carrier chip has a 1-μm-thick superconductive niobium pattern including the coplanar transmission line (tl) that provides the high frequency connection to the sampler chip.

The 5–20 μm spacing between the sampler chip and the carrier chip, which is typical for the flip-chip bonding technique, makes it possible to obtain much lower inductance leads to the sampling circuit than would be possible using traditional bond wires. This advantage is increasingly important as the signal frequency goes up into the GHz range, since the high inductance of traditional bonding wires leads to a significant parasitic impedance at such high frequencies. For this reason the flip-chip bonding technique is a good alternative to wire bonding for high frequency interconnections.

It should be noticed that hysteretic Josephson junctions were recently fabricated by Virshup *et al.*[12] using high temperature superconductors. By utilizing such junctions it will be possible to operate superconductive samplers at higher temperatures in the future.

II. THE SAMPLING CIRCUIT

The superconductive oscilloscope utilizes a fast spike-like electrical pulse of approximately 5.5 ps full width at half-maximum (FWHM) which strobes the electrical signal under measurement one point at a time as shown in Fig. 2. The high frequency signal has to be identically repeated many times in order to scan the entire signal, and for this the repetition frequency can be much lower than the signal frequency. We use a 10 kHz repetition rate.

The amplitude of the signal is determined by means of a summing comparator with a threshold level I_c. The comparator is fed by the signal $I_{\text{signal}}(t)$, the strobe pulse $I_{\text{strobe}}(t_p)$ occurring at time t_p, and a feedback current $I_{\text{fdbk}}(t_p)$. Because the signal is repeated, the feedback circuit can be made as an integrating counter that will adjust the feedback current $I_{\text{fdbk}}(t_p)$ so the comparator will switch to its voltage state (at $I=I_c$) with 50% probability. The following threshold condition is then fulfilled at the time t_p of the signal

$$I_c=I_{\text{signal}}(t_p)+I_{\text{strobe}}(t_p)+I_{\text{fdbk}}(t_p). \tag{1a}$$

Since the threshold level (I_c) as well as strobe amplitude (I_{strobe}) are fixed, the signal can be determined from

$$I_{\text{signal}}(t_p)=-I_{\text{fdbk}}(t_p)+\text{const.} \tag{1b}$$

It is important to notice that in this way only one point in the signal is determined when the feedback current has been set by the feedback circuit. After that the position (t_p) of the strobe current relative to the signal can be changed and a new amplitude value can be determined. By scanning

[a]Presently at the Electrotechnical Laboratory, 1-1-4 Umezono, Tsukuba Science City, 305 Ibaraki, Japan.

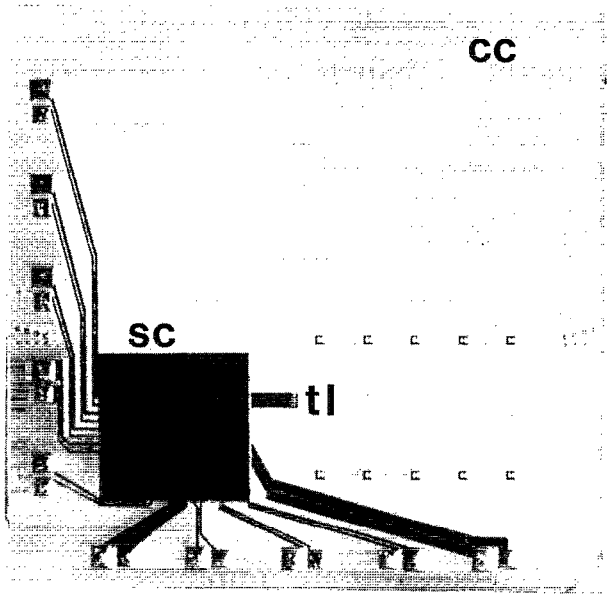

FIG. 1. The sampler chip (SC) flip-chip bonded to the top of the carrier chip (CC). The end of the coplanar transmission line (tl) with its three connection pads can be seen to the right of the sampler chip.

the strobe pulse in time relative to the signal the entire high frequency signal will be measured.

Figure 3 shows the current voltage characteristic of a Josephson junction based interferometer, to illustrate how it can be used either as a comparator gate or a pulse generator. In the zero voltage state the current injected into the interferometer is less than the critical current I_c. If the current exceeds I_c the junction will switch to the voltage state and stay there until the current is lowered following the quasiparticle curve (QP). In this mode the interferometer works as a threshold detector. In the pulse generator mode, we benefit from the fact that the switching time from the zero voltage state to the voltage state is only a few picoseconds.

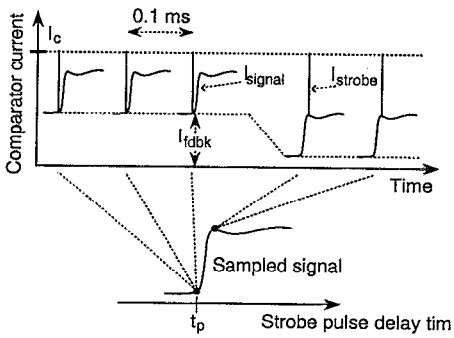

FIG. 2. The sampling principle. The same signal is shown repeated several times with the strobe-pulse superimposed on it. The elapsed time between each signal repetition is 0.1 ms, which is much longer than duration of the signal itself. The feedback current $I_{fdbk}(t_p)$ is the current that must be added to make a Josephson junction based comparator gate switch into its voltage state from its zero voltage state. Since the comparator is hysteretic it stays in the voltage state until it is reset by a control current. By detecting whether the comparator gate is switched or not, the feedback current can be adjusted accordingly. The threshold level of the comparator is I_c.

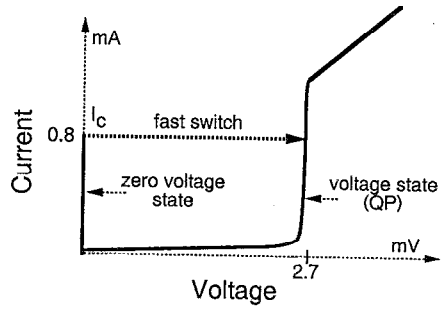

FIG. 3. The current–voltage characteristic of a Josephson junction based interferometer. If the current injected into the interferometer exceeds the critical current I_c the junctions in the interferometer will switch from the zero voltage state to the nonzero voltage state. In this way it can be used as a threshold detector. Because the switching time from the zero voltage state to the voltage state is in the order of picoseconds, the interferometer can also be used as a fast pulse generator.

The sampler circuit we use is part of a larger scientific chip, SCT-2, developed in 1983 at the IBM Research Center, Yorktown Heights using the $Nb/Nb_2O_5/Pb$ technology with a junction current density J_c of 4 kA/cm^2 and a capacitance to critical current ratio C'/J_c of 2.5 pF/mA. The bandwidth of the sampler is determined by the dynamics of the Josephson junctions together with their embedding circuits[9] and limited to about 55 GHz. In Fig. 4 it is seen that the sampler strobe pulse generator consists of two Josephson junctions (JJ1, JJ2) in the interferometer configuration, plus a third junction (JJ3). This scheme was originally proposed by Faris *et al.*[1] The strobe pulse starts when the interferometer (JJ1, JJ2) switches to the voltage state. The switch creates a fast rising current ramp that picoseconds later will make the third junction (JJ3) also switch to its voltage state. The junction JJ3 will block the rising current and cause a descending ramp, so that a spike shaped pulse is generated.

The comparator—which acts as the latching sampling gate—is a two junction (JJ4, JJ5) interferometer with the signal, strobe pulse, and feedback currents inductively cou-

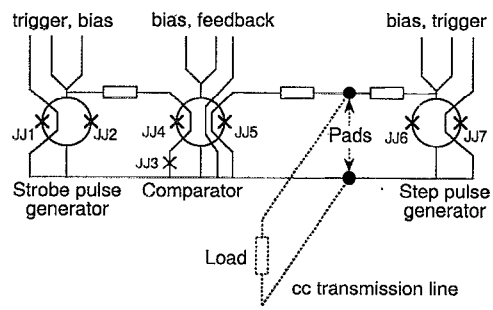

FIG. 4. Diagram of the sampling circuit made at IBM Yorktown Heights in 1983 by the Nb/Pb technology. From left to right the diagram shows: (*) The strobe-pulse generator, made from the interferometer (JJ1,JJ2) that generates the rising pulse edge, and a single junction (JJ3) that provides the descending edge. FWHM of the strobe pulse is about 5.5 ps. (*) The comparator which consists of one interferometer (JJ4,JJ5) with the strobe pulse, the signal, and the feedback current inductively coupled to it. (*) The flip-chip bonding pads that connects the sampler to an external transmission line. (*) The step-pulse generator (JJ6,JJ7) which generates pulses with 5.6 ps rise time (10%–90%).

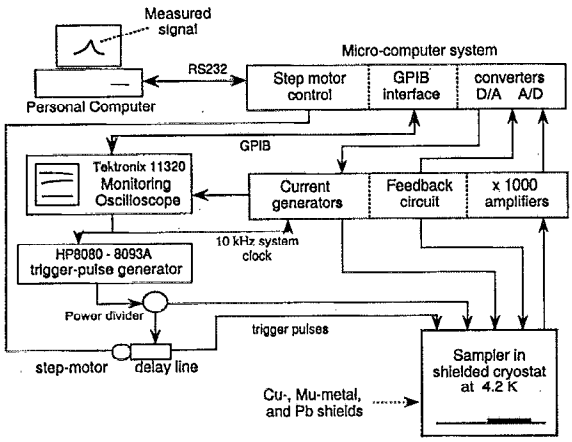

FIG. 5. Schematic diagram of the Josephson sampling oscilloscope. The sampler circuit and the carrier chip are at liquid helium temperature (about 4.2 K) in a shielded cryostat while the control electronics are at room temperature. The computer controls all functions of the sampler except the level of the trigger pulses from the HP8080/8093A to the strobe-pulse and step-pulse generators. The Tektronix oscilloscope supplies the 10 kHz system clock and is used to monitor the signal to and from the sampler circuit. The feedback circuit works as an integrating counter and automatically adjusts the feedback current after the appropriate working points have been set by the computer.

pled to it. The inductive coupling provides a dc isolation between the signal and the comparator. The input terminals to the comparator are lined up with holes in the SiO protective layer of the SCT-2 chip. When the SCT-2 chip is flip-chip bonded to the carrier chip, the input terminals are connected to the high frequency coplanar transmission line. As also shown in Fig. 4 a step-pulse generator on the SCT-2 chip is connected to the transmission line. In this way it is possible to generate a step pulse that will propagate down the transmission line to the load and subsequently return to the sampling gate to be measured. By using the step-pulse generator in this scheme, the instrument works as a fast and sensitive time domain reflectometer (TDR) where the time difference between the outgoing step pulse and the incoming signal is roughly determined by twice the propagation time for the pulse on the transmission line.

III. THE CONTROL ELECTRONICS

Figure 5 shows the setup that includes the superconductive sampler chip in a cryostat cooled to 4.2 K by means of liquid helium. The cryostat is of the two Dewar vertical type with the outer Dewar for liquid nitrogen at 77 K, and the inner Dewar at liquid helium temperature, 4.2 K. Two liters of liquid He allows for 8 h of operation.

The electronics includes:

* A PC computer with a standard serial RS232 interface connected to a microcomputer system with analog-to-digital (A/D) converters, strobed digital-to-analog (D/A) converters, delay line step-motor control, and a general purpose interface bus (GPIB) parallel interface. The GPIB is connected to the Tektronix (11320) programmable analog oscilloscope which monitors all signals to and from the sampler circuit. The Tektronix oscilloscope also provides the 10 kHz system clock that determines the repetition rate of the signal to be measured.
* 12 bit strobe resettable D/A converters with the output fed into 15 kHz low pass filtered current generators that in turn are connected to the bias lines of the interferometers on the sampler chip.
* $\times 1000$ voltage amplifiers that amplify the voltage across the Josephson junction interferometers. When a Nb/Pb Josephson junction switches to its voltage state the voltage across the junction is only 2.7 mV. The amplifiers are therefore necessary to isolate the Josephson junction interferometers and to provide a voltage level compatible with the subsequent A/D converters and the feedback circuit.
* 16 bit A/D converters with the inputs connected to the outputs of the $\times 1000$ amplifiers. By using D/A and A/D converters the current voltage characteristic (IV curve) and the critical current versus feedback current $[I_c(I_{\mathrm{fdbk}})]$ curve can be read in to the computer. Afterwards we use a computer algorithm to automatically determine the optimal working points for the strobe-pulse generator, the comparator, and the step-pulse generator, respectively.
* A feedback circuit based on an integrating counter and a current generator. The time constant of the integrator and the switching probability of the comparator can be chosen independently.
* A HP8080 pulse generator that provides 650 ps FWHM time-synchronized trigger pulses for the sampler strobe pulse generator and the step generator.
* A 1000 ps delay line with a step-motor control allowing a time resolution of ~ 0.2 ps. The delay-line length (1000 ps) determines the lower measuring frequency of 2.0 GHz. The delay is computer controlled.

The microcomputer system as well as the low noise bias, feedback and amplifying electronics are made using standard half size 19 in. rack with plug-in units. The modular construction enables us to modify the setup according to the experiment, as different experiments often require a different number of current generators amplifiers, etc. Because the plug in units are standardized, servicing is easy.

The PC program that runs the sampler has been designed to perform the following functions:

* Automatic measurement of the *IV* curves and critical current versus feedback current for the gates on the sampler chip.
* Automatic setting of the repetition frequency, the monitoring oscilloscope, and the sampler-gates bias currents.
* For a measurement of a high frequency signal the software includes: use of cursors, zoom, digital low pass filtering–smoothing, and a Fourier-transform routine.

Data are stored to a disk drive as sequential ASCII files that can be transferred to other types of programs (e.g., spreadsheets).

IV. FLIP-CHIP MOUNTING

As shown in Fig. 1 the superconducting sampler chip (SC) is flip-chip bonded to the larger carrier chip (CC). The CC contains a niobium pattern for connections to the controlling electronics and the coplanar transmission line. The transmission line in turn provides the high frequency connection between the SC and a device under test

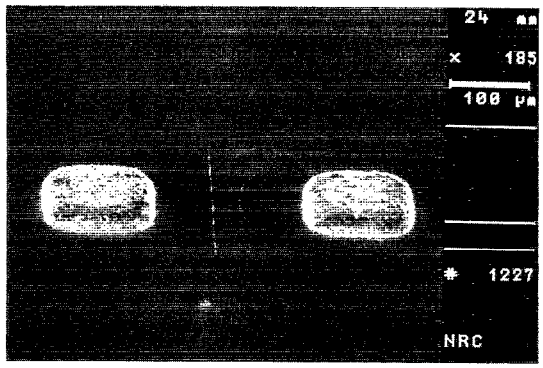

FIG. 6. The 140 μm $\times$140 μm copper bonding pads on the carrier chip before deposition of Rose's metal. These bonding pads are about 20 μm high and they are used when the sampler chip is soldered to the carrier chip.

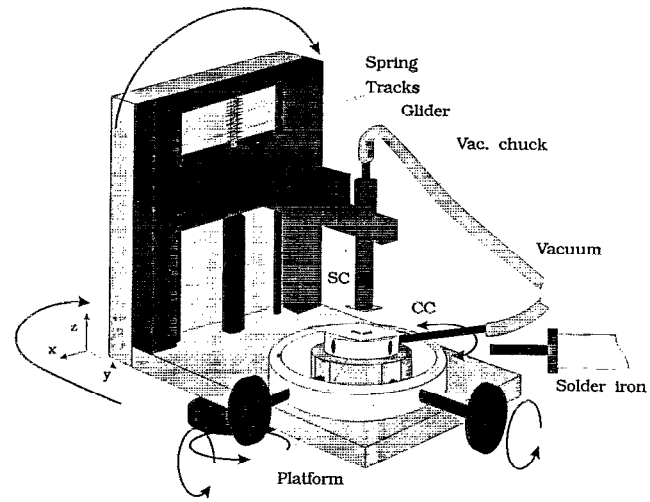

FIG. 7. The flip-chip bonding machine consists of a platform that can be moved in the x and y directions and a chuck that moves in the z direction perpendicular to the platform. The carrier chip (CC) is mounted on the platform and the sampler chip (SC) is placed on the chuck. Both chips are held by a vacuum that is controlled by a gate valve with a lever. During bonding the whole setup can be rotated around two axes to allow inspection of the space between the two chips from different sides. Heating of the platform and the carrier chip for soldering is done by a soldering iron inserted into the platform. Bonding can be performed with an accuracy of better than 10 μm.

(DUT). The 1×1 in.^{2} CC substrate is of 0.8-mm-thick sapphire. The SC has contact pads for the controlling currents along the edges and the pads for the transmission line at the center of the chip. The edge pads are 100 by 280 μm^2 and the two pads at the center shown in Fig. 6 are 140 by 140 μm.^{2} In total we connected 22 pads from the SC to the CC. After flip-chip bonding the sampler chip, a DUT chip can be bonded to the three pads at the end of the transmission line.

The contact resistance which needs to be less than about 0.1 Ω depends on the mechanical quality of the interface between the bonding pads and on the materials used. If we simply press the SC and the CC together, the contact resistance is determined by the contact pressure and the nonuniformity of the heights of the carrier chip pads. For this reason soft-metal type contacts were used which allowed the automatic leveling of the contacts by applying pressure. Using this technique the contact resistance was always below 0.1 Ω measured by the two point method.

Commercial systems for aligning and bonding are available[13] but are expensive and are mainly dedicated to semiconductor industry applications. We chose to develop the much simpler flip-chip bonding machine shown in Fig. 7. The setup consists of two parts: (1) a $\times$20 stereo microscope and (2) the machine itself. The carrier chip is held by a vacuum face upwards on a platform which can be moved in the x and y directions with adjustment screws and can be rotated in the x–y plane. The sampler chip is placed face down on a vacuum chuck directly above the center of the platform. The chuck is fixed in the x–y plane but can be moved perpendicular to the platform surface along the z axis. The chuck is forced down towards the platform by a spring and held up by an adjustable screw so that the two chips can be held very close together during the process of alignment. The whole setup can be turned in two directions, and viewing through the microscope can be done from different angles. When a thin round glass fiber is covered with a thin layer of gold it works as an excellent round mirror, and alignment of the contact pads to the transmission line can be done by holding the glass fiber between the closely spaced chips while viewing through the microscope. Along the edges of the SC the mirror image of the edge contact pads of the SC can also be seen in the Nb lines on the CC. This is an extra help during the alignment procedure, and alignment can be carried out with an accuracy of better than 10 μm. After alignment the SC is lowered down onto the CC by turning a screw and the vacuum is removed from the chuck. The SC is then forced down on the CC by the spring. If additional pressure is needed the upper and lower part of the bonding machine can be pressed together by hand. The spring applies a pressure of 200–400 g, but usually about 1000 g is needed if the contact pads are not soldered but merely held together by the soft materials on the contact surfaces.

In early experiments solder bumps were placed on the contact pads of the CC by solder dipping using eutectic Pb/Sn as in Ref. 11. Before the dip soldering the Nb pads were coated with a 2 μm copper layer. The bumps were about 30 μm high before the bonding but shrunk to less than 15 μm during bonding. To ease bonding and to reduce the needed pressure the height (typical spread $\sim$3 μm) of the solder bumps could be equalized by pressing a thick plane glass plate onto the pads. The bump deformation could be watched through the glass plate and it was easy to see when all bumps had the same height.

Even though this technique of pressing the SC and CC together worked, it turned out to be not fully reliable during cooldown. To solder the SC and CC together, we changed the procedure for making the contact pads on the CC. Because the original CC was made of sapphire while the SC is on a silicon substrate, soldering cannot be done due to the difference in thermal expansion coefficients (the bonding would crack during cooldown to liquid He tem-

peratures). Therefore 1×1 in.^{2} substrates were cut out from 0.2 mm Si wafers and used as CCs (thicker wafers should preferably be used to avoid bending and breaking). After this, about 20 μm high copper pads were electrochemically deposited on the CC through a photoresist mask in an acid copper-sulphate solution (20 g cryst. $CuSO_4+5H_2O$, 2.1 ml (95%) H_2SO_4, 100 ml H_2O) applying a current density of 30 mA/cm^2 through the photoresist mask. The electroplated layer had a rather rough surface and was not 100% homogeneous. It was smoothened by gently grinding the CC face down on a fine grinding stone (Hard Arkansas Oilstone HB5). After cleaning, dip soldering was carried out in a low melting point texture, Rose's metal (50% Bi, 25% Sn, 25% Pb), with the melting point of 85–90 °C. This results in sandwich type contacts with equal height and a top layer of solder with a low melting point.

The bonding machine was fitted for soldering with a platform of copper, which is thermally decoupled by a fiberglass plate. Furthermore a hole was drilled in the platform to fit a copper rod that in turn fits into a temperature regulated solder iron. In this way the platform and the CC can be heated up to a controlled temperature. The two chips are first aligned without touching and without heating the platform. When alignment is completed the SC is levitated well above the CC and the solder iron is turned on. After the melting point of the solder is reached, the SC is gently lowered down and pressed onto the CC. The sudden thermal contact causes the solder to solidify instantly and, to avoid further heating of the SC, the sandwich is quickly removed from the bonding machine. This method gives a bonding that stands repeated thermal cycling between 300 and 4.2 K.

V. EXPERIMENTAL RESULTS

Because the soldering procedure using a silicon CC was introduced at a later stage in the project the following data were obtained using sapphire substrates without soldering.

A. A test signal

Figure 8 shows a test signal from the step-pulse generator on the sampler chip itself without connection to the coplanar transmission line. The rise time of this 220 μA signal was 5.6 ps (10% to 90%), and the bandwidth of the instrument can be estimated to be

$$1/\pi/5.6\ \text{ps}\sim55\ \text{GHz}.$$

B. The sampler as a TDR instrument

We connected the comparator and the step-pulse generator to a coplanar transmission line with nominally 25 Ω impedance. Before connecting a device to the transmission line, we investigated the quality of the transmission line itself. For this purpose a simple short circuit was placed on the transmission line, 4.0 mm away from the sampling circuit. The measured signal is shown in Fig. 9. Because the transmission line was short circuited, the step pulse was reflected as a negative going pulse at the end of the

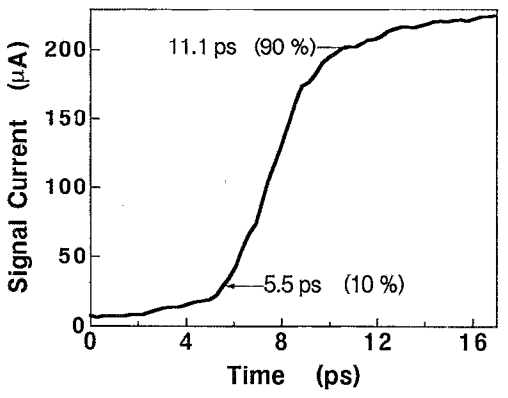

FIG. 8. Measured step pulse from the step-pulse generator. In this case no transmission line was connected to the sampler. The signal rise time was 5.6 ps and the amplitude 220 μA. From this pulse we determine the bandwidth of the superconductive sampler to be 55 GHz.

transmission line end. Adding the negative reflection to the step pulse, the signal amplitude becomes zero when the negatively reflected step returns to the sampler. The amplitude of the main pulse was 45 μA and the time from the foot of the rising part of the pulse to the point where the pulse starts decreasing from its maximum is 52.5 ps. These 52.5 ps are twice the propagation time for the pulse on the transmission line. Some undershoot at the end of the pulse and a tail of damped oscillations with a 23 ps period time can be seen. The rise time of the pulse is about 20 ps, a value much slower than the intrinsic rise time of the step-pulse generator.

VI. DISCUSSION

A. The transmission line

Since the comparator is in parallel with the transmission line, the fast step-generator pulse is divided between

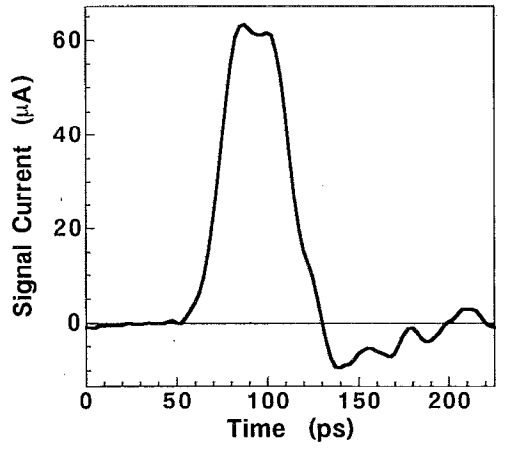

FIG. 9. Measured pulse, obtained by connecting the step-pulse generator to a nominally 25 Ω coplanar transmission line with a short circuit 4.0 mm from the sampler. The resulting pulse is the sum of the step pulse transmitted down the transmission line and the same step reflected negatively at the short circuit. The time from the foot of the rising edge to the beginning of the descending flank is thus the traveling time for the step pulse back and forth the transmission line. The relatively slow 20 ps rise time of the rising flank is probably due to a parasitic capacitive load of the transmission line on the sampler circuit.

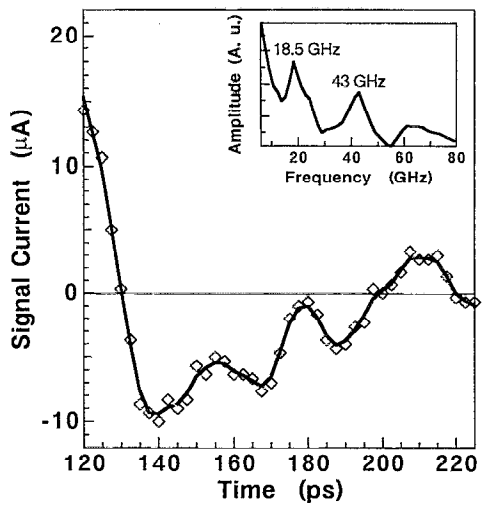

FIG. 10. The tail of the main pulse from Fig. 9 shown in detail. The original data, shown as diamonds, have been smoothed by a running average. The effect is a low pass filtering with improved current resolution. The tail can be seen to consist of a slowly varying background rising from multiple reflections of the main pulse, and a damped 23 ps oscillation. The 23 ps oscillations might be formed from a series resonance between the leads to the transmission line and the capacitance of the transmission line relative to the sampler. The inset shows the Fourier transform of the original data. The frequency of 18.5 GHz corresponds to the multiple reflections of the main pulse and the 43 GHz peak corresponds to the 23 ps oscillating tail.

the comparator and the transmission line. This leads to a suppressed signal amplitude compared to the test signal, as shown in Fig. 9. From the slow rise time we conclude that the impedance of the transmission line is mainly capacitive. This is not surprising since the sampler chip is only about 10 μm above the transmission line and the coplanar transmission line has an open structure. Both effects can be expected to produce an extra stray capacitance. The stray capacitance ($C_{SC,CC}$) of the transmission line to the ground plane of the sampler chip is 1–4 pF [calculated by the area of the transmission line facing the SC, the 10–15 μm spacing between the chips, and the gap partially filled with SiO ($\epsilon_r=5$)]. In order to obtain the shorter rise time of about 6 ps which is typical for the step-pulse generator the relatively large stray capacitance of 1–4 pF should have been reduced. We used coplanar transmission lines because they are easy to fabricate but a drawback is their open structure. A smaller stray capacitance could have been obtained either by using a closed structure transmission line, e.g., by fabricating a microstrip line with the ground plane facing the sampler chip or by placing the sampler circuit at the very edge of the sampler chip.

Figure 10 shows the pulse end and the oscillation in detail where the data have been low pass filtered by a three point triangular running average. This procedure normally improves current resolution at the cost of bandwidth, but in this case, by over sampling the signal, the low pass filtering does not effectively lower the bandwidth. The inset in Fig. 10 shows the Fourier transform of the original signal data. Two frequencies are clearly visible; the lower one at 18.5 GHz which is the result of multiple reflections between the sampler/transmission line connection, and the higher one at 43 GHz which corresponds to the 23 ps tail oscillation. The 23 ps tail of oscillations in Figs. 9 and 10 is probably due to a resonance between the inductances in the bonding to the transmission line (L_{bond}), combined with the 1–4 pF stray capacitance of the transmission line to the sampling circuit. A value for the parasitic inductance L_{bond} using the flip-chip bonding technique can only be estimated very roughly from the height of the Pb/Sn bonding pads on the carrier chip. By assuming that the signal current is confined to the edges of the contact pads due to the skin effect we can use $\mu_0/4\pi$ as the *intrinsic* inductance. The kinetic inductance of the Cooper pairs[14] in the superconductor and the geometric inductance of the contact pads should also be added, but the intrinsic pad inductance can still be used as an estimate of the lowest value

$$L_{bond} > 2\times 15\mu m\times\mu_0/4\pi = 3 \text{ pH}.$$

These estimates of stray capacitance and parasitic inductance leads to an estimated $L_{bond}C_{SC,CC}$ time constant of 10–20 ps or greater, in fairly good agreement with the measured tail oscillation time of 23 ps.

B. Noise

The cryostat is screened by Cu and mu-metal shields (Vacuumschmelze). Since Josephson junctions are sensitive to magnetic fields it is essential to have a good magnetic shielding. We found for that two concentric mu-metal cylinders plus a cylindrical 8-cm-diam superconductive Pb shield around the holder for the sampler chip and transmission line gave good magnetic shielding and long term stability for the measurement. One drawback of the superconductive shield is that the shield itself may trap magnetic flux and thus disturb the Josephson junctions. Slow cooling of the sampler chip and shield, however, reduces the thermoelectric currents that generate magnetic fields and in this way the trapped flux can be reduced to an acceptable level.

Due to the latching nature of the Josephson junctions, noise conducted via the control lines to the strobe pulse generator only affects the amplitude of the strobe pulse slightly. A more severe effect is that the noise alters the trigger level of the strobe pulse generator and hence generates time jitter of the strobe pulse relative to the signal. Jitter, together with the feedback circuit coupled to a threshold detector, will impose an ultimate time resolution that can be understood in the following way. The feedback circuit is set to a 50% switching probability and if we consider a signal which is a short pulse, the pulse can only be detected if more than 50% of the strobe pulses coincide with it. If the switching probability cannot reach 50% the feedback circuit will indicate a zero signal. Such as pulse will never be detected. Assuming a Gaussian distribution of the strobe jitter relative to the signal we get

$$P_{switch}=0.5=\text{erf}(x) \quad \text{with } x=\Delta t_{min}/(\sigma_{jit}2\sqrt{2}), \quad (2a)$$

where Δt_{min} is the minimum detectable pulse width and σ_{jit} is the jitter spread. Using a standard table we get

$$\Delta t_{min}\sim 1.36\sigma_{jit}. \quad (2b)$$

Equation (2b) shows that the jitter imposed time resolution in a system with a threshold detector is slightly larger than the strobe jitter spread. In early experiments the noise was too large, and as a consequence the time resolution was jitter limited to about 10 ps. By introducing cooled attenuators for the trigger lines and by using the same trigger pulse divided for the signal generator and strobe pulse generator trigger, respectively, the time resolution of about 5 ps was reached. In our equipment, it is not possible to obtain a better time resolution than 5 ps because this limit is set by the width of the strobe pulse.

By doing repeated measurements on the signal in Fig. 8 and calculating the spread in the measured signal value $\sigma[i_{\text{signal}}(t_p)]$, a clear correlation between the pulse edge steepness (μA/ps) and the spread in the measurement was found

$$\sigma[i_{\text{signal}}(t_p)]=0.5\ \mu\text{A}+1.0\ \text{ps}\times di_{\text{signal}}(t_p)/dt. \qquad (3)$$

This means that the spread in a measured signal value is 0.5 μA if the signal has no time variation and the spread rises in proportion to the time derivative of the signal. Assuming a linear relation between the signal spread and the jitter spread, the jitter spread can be inferred to be 1.0 ps from Eq. (3). Inserting this value into Eq. (2b) the ultimate jitter imposed resolution would be about 1.5 ps. This value is (and should be) well below the 5 ps strobe pulse width, but jitter still deteriorates the accuracy of a measured signal value according to Eq. (3).

ACKNOWLEDGMENTS

The authors would like to greatly acknowledge Dr. S. Sakai and Dr. N. F. Pedersen for their kind help and many encouraging discussions. This work was supported by the Danish SNF and STVF (J. No. 5.17.16.37+5.17.1.1.20) and Broedrene Hartmanns fond.

[1] S. M. Faris, Appl. Phys. Lett. **36**, 1005 (1980).
[2] D. B. Tuckerman, Appl. Phys. Lett. **36**, 1008 (1980).
[3] S. M. Faris and N. F. Pedersen, Physica B **108**, 1087 (1981).
[4] P. Wolf, B. J. Van Zeghboeck, and U. Deutsch, IEEE Trans. Mag. Mag. **21**, 226 (1985).
[5] S. Sakai, H. Akoh, and H. Hayakawa, Jpn. J. Appl. Phys. **22**, L479 (1983).
[6] S. Sakai, H. Akoh, and H. Hayakawa, Jpn. J. Appl. Phys. **23**, L610 (1984).
[7] H. Akoh, S. Sakai, and S. Takada, Phys. Rev. B **35**, 5357 (1987).
[8] H. Akoh, S. Sakai, A. Yagi, and H. Hayakawa, Jpn. J. Appl. Phys. **22**, L435 (1983).
[9] P. Bodin, Ph.D. thesis, 1991 (unpublished).
[10] J. Bindslev Hansen, A. Davidson, M. Brady, and N. F. Pedersen, Jpn. J. Appl. Phys. **26**, 1603 (1987).
[11] M. J. Brady, A. Davidson, Rev. Sci. Instrum. **56**, 7 (1985).
[12] G. F. Virshup, M. E. Klausmeister-Brown, I. Bozovic, and J. N. Eckstein, Appl. Phys. Lett. (submitted).
[13] Research Devices, 121 Ethel Road West, Piscataway, NJ 08854.
[14] T. Van Duzer and C. W. Turner, *Principles of Superconductive Devices and Circuits* (Elsevier–North Holland, New York, 1981).